REMOTE SENS. ENVIRON. 49:212-223 (1994)

Photographic and Videographic Observations for Determining and Mapping the Response of Cotton to Soil Salinity

C. L. Wiegand, J. D. Rhoades,† D. E. Escobar,* and J. H. Everitt**

Better ways are needed to assess the extent and severity of soil salinity in fields in terms of economic impact on crop production and effectiveness of reclamation efforts. Procedures to help meet these needs were developed from soil salinity, plant height and boll counts, and digitized color infrared aerial photography and videography acquired during midboll set development stage for four salt-affected cotton (Gossypium hirsutum, ***L.) fields in the San Joaquin Valley of California. Unsupervised classijication procedures were used to produce seven-category spectral maps*** by ***field. Regression equations were developed from salinity measurements in the surface 30 cm (EC1)*** at ***100-200*** sample sites ***per field*** and the photography and videography digital counts at those same sites. ***The equations were used to estimate the salinity of each of the approximately 100,000 pixels per field, and the salinity categories*** corresponding ***to the spectral ones were mapped. The spectral classification maps and the estimated salinity maps corresponded well. Boll counts, made at about 20 sites perjield, were converted to lint yield and regressed on NDVl from both the photography and videography; the correlation coefficient*** (r) ***was 0.72 for video and 0.73 for the photographic data. Lint yields decreased by 43 ± 10 kg*** ha^{-1} ***per*** $dS\,m^{-1}$ ***increase in ECl, or $52 ± 12*** ha^{-1} ***at current market prices. Our results illustrate very practical ways to combine image analysis capability, spectral observations, and ground truth to map and quantify the severity of soil salinity and its effects on crops.***

*USDA / ARS, Subtropical Agricultural Research Laboratory, Remote Sensing Research Unit, Weslaco, Texas

† USDA / ARS, U. S. Salinity Laboratory, Riverside, California

Address correspondence to Craig L. Wiegand, USDA /ARS, Remote Sensing Research Unit, 2413 E. Hwy. 83, Weslaco, TX 78596-8344.

Received 25 February 1993; revised 20 April 1994.

INTRODUCTION

Soils are termed saline or salt-affected when the concentration of salts in the root zone exceeds 4 $dS\,m^{-1}$ (Richards, 1954). Such soils comprise 19% of the 2.8 billion hectares of arable land worldwide (Szabolcs, 1989). Saline soils occur naturally in arid and semiarid climates from weathering of indigenous minerals (Tanji, 1990) but are more important economically where irrigation is practiced to produce crops (Carter, 1975). Nonsaline irrigated soils can become saline in time when leaching is insufficient to remove salts applied in the irrigation water, or drainage is insufficient to prevent a saline water table from rising within about 1.5 m of the soil surface. Downstream irrigation projects are jeopardized because return flow of drain water to river systems invariably contains more salt than when diverted.

Information on the extent and severity of soil salinity is needed to engineer water delivery and drainage improvements. Once reclamation efforts are underway, methods are needed to monitor the effectiveness of reclamation or amelioration. Aerial photography (Myers et al., 1966) and Apollo 9 (Wiegand et al., 1971) and Skylab (Everitt et al., 1977) 1:3,000,000-scale space photography as well as Landsat multispectral scanner (MSS) 1:250,000-scale imagery (Sharma and Bhargava, 1988) have been used to distinguish saline from nonsaline soils and vegetation. Everitt et al. (1988) used narrowband videography to detect and estimate the aerial extent of salt-affected soil in southern Texas. Wiegand et al. (1991; 1992) related three bands of video and the three HRV scanner bands of the French polar-orbiting satellite SPOT-l to lint yield and percent ground cover of cotton in a single I5-ha salt-affected field; yield and plant cover were estimated equally well from vegetation indices (Kauth and Thomas, 1976; Richardson and Wiegand, 1977; Tucker, 1979) from both systems.

0034-4257/94/$7.00

655 Avenue of the Americas, New *York, NY 10010*

Table 1. **Size** and Designations of Fields, Sampling Pattern and Number of Samples, and Range, Mean, and Standard Deviation of Electrical Conductivity of Saturation Extracts (EC1) from the Surface 30 cm of Soil for the Fields Studied

Field (1.D.)	*Size (ha)*	*Sample Transects (No.)*	*Transect Spacing (m)*	*Sample Spacing Within Transects (m)*	*Samples Taken (No.)*	*EC1*		
						Range	*Mean (dS m^{-1})*	*S.D.*
2c	13.7	13	23	15 or 16	198	o-17	2.25	3.3
3c	12.5	14	24	13 to 6	149	O-25	3.07	4.0
9A	16.1	13	31	13	169	o-17	4.29	3.3
9E	12.4	6	50	17	102	O-27	7.65	5.3

The widely used VI include the greenness vegetation index (GVI) (Kauth and Thomas, 1976; Jackson, 1983) that is calculated from observations in three or more bands, and the normalized difference vegetation index (NDVI) (Tucker, 1979) that is calculated from observations in a visible red (Red, 600-700 nm) and a near-infrared (NIR, 750-1350 nm) band.

Wiegand and Richardson (1984; 1987; 1990) developed spectral components analysis (SCA) to help interpret vegetation indices in terms of crop growth and yield and the underlying canopy processes such as light interception and evapotranspiration. Briefly, principles implicit in SCA include: 1) Plants integrate the soil and aerial environments experienced and express their responses to stresses through the canopies achieved; 2) high yields obtain only when growing conditions permit canopies to develop that fully intercept sunlight during the reproductive stage of development; (3) commercially successful producers use recommended cultivars, planting rates and configurations, fertilization, insect and disease control and other practices that permit the needed full canopies to develop; 4) vegetation indices, such as NDVI, are measures of the photosynthetic size (amount of photosynthetically active tissue) of the canopies; and 5) stresses reduce yields proportional to the reduction in photosynthetic size and duration I persistence of the canopies during production of the salable plant parts that constitute economic yield. Thus effect of single or multiple stresses on economic yield can be interpreted through spectral observations that capture their effect on photosynthetic size of the canopies.

The SCA relations for crop response to soil salinity are expressed by

$$\text{Yield(NDV1)} = \text{Yield(EC)} \times \text{EC(NDV1)} \quad , \qquad (1)$$

where, for cotton, yield is lint yield (kg ha-l), EC is the electrical conductivity (dS m^{-1}) of water extracts from soil samples taken from the root zone of the crop, and NDVI is calculated from digital responses in NIR and Red wavelengths. Axiomatically, for the Eq. (1) relationships to be strong, the effects of soil salinity have to dominate the other sources of variation (cultivars, soils, carryover and current year's tillage and fertilization) and the error in sampling. For sugarcane, Wiegand et al. (1993) reported that stalk yields decreased 23.8 $\pm$ 3.8 metric tons ha-' per unit increase in EC and that stalk yield related more closely to NDVI (r= 0.82) than to EC (r = – 0.77).

In this study we report on soil salinity, plant height and cover, and digitized color infrared photography and multispectral narrowband videography observations obtained from four cotton fields in the San Joaquin Valley of California. The objectives were to a) determine the interrelations among plant, soil salinity, and spectral observations by field, b) jointly use those relationships and image analysis techniques to map the severity and spatial distribution of soil salinity in cropped fields, and c) interpret results in terms of the economic costs of salinity. Our hypotheses were that the spectral observations sense plant growth and yield responses to soil salinity and can help map and quantify the extent and severity of soil salinity in crop fields. Successful accomplishment of the objectives would provide illustrative relations between spectral observations and soil salinity, and demonstrate another way to determine the extent and severity of soil salinity or, alternatively, to monitor the progress of reclamation.

METHODS

Field Sampling

Four commercial fields of cotton (Gossypium hirsutum L.) within a 39 km^2 intensive study area in the San Joaquin Valley of California (Lesch et al., 1992) were used. The field designations, transect spacing, sample intervals along the transects, and salinity of the surface 30 cm of soil are summarized in Table 1. Sampling strategy had been preplanned to provide at least 100 sample sites per field. Intervals between sample sites were determined by pacing, after which coordinates were determined ($\pm$ 0.1 m) with a Zeiss' DME theodolite system.

Soil samples were taken from the O-2 cm, O-30 cm, and 30-60 cm depths at three positions within about

[1] **Trade names are included for the benefit of the reader and do not imply endorsement of nor preference for the mentioned product by the U.S. Department of Agriculture**

***Table 2.* Systems Used, Wavelengths of Each System, and Nominal Pixel Width**

System			
Photography			
Film Response	Digitizing Filters	Videography	Band (Name)
	Wavelength Interval (nm)		
750-900	610-730"	845–857[b]	Near-infrared
600-700	515–570[a]	644-656	Red
500-600	390–480[a]	543-552	Green
	Pixel Width (m)		
1.0-1.2		3.4	

[a] Filters used on Eikonics camera to digitize the Kodak Aerochrome infrared film 2443 positive transparencies.
[b] A 0.5 neutral density filter was also used on an NIR-filtered camera.

0.5 m of each **sample** site, using a Lord tube, and composited by depth. Electrical conductivity of the saturated-soil extracts (EC_e, $dS\,m^{-1}$) was determined by the procedures of Rhoades (1982). Electrical conductivities were designated ECO, ECl, and EC2 for the O-2 cm, O-30 cm, and 30-60 cm depths, respectively.

Plant height (PH, cm), percent bare area (PBARE), and number of bolls were the plant observations recorded. Plant height and PBARE were determined and recorded at all sites, but bolls m^{-2} was determined at only 17-20 sites per field. If plants were absent at the sample site, the height was recorded as zero and the range in plant height within a 10 m x 10 m area surrounding the sample site was measured and recorded. PBARE was estimated visually as percentage of 10-m lengths of row, surrounding the sample site, that was devoid of plants. Thus PBARE recorded as zero meant a full stand of plants was present. Bolls m^{-2} was expanded to kg lint ha^{-1} based on 600 bolls per kg lint (Wiegand et al., 1992). Plant and soil sampling required 1 day per field. All samples were acquired between 27 July and 5 August 1989.

Soils and agronomic practices differed among fields. In field 9E the seed had been planted on top of the bed in a shallow furrow between two miniridges toward each edge of the bed. In the other fields, the miniridges were absent. Row spacing in all fields was approximately 1 m.

Spectral Data

The photography and videography were acquired on 31 July 1989, with the systems mounted in a Aero Commander aircraft. Twelve-inch format aerial photography using Kodak Aerochrome infrared 2443 film was acquired of the entire study area from I500 m above ground level between approximately 1100 h and 1300 h Pacific Standard Time. Aperture setting was F8 and shutter speed was 1 I500 s. Red plastic sheeting 0.70 m wide and 3.0 m long was used to form "plus sign" markers in three corners of each field. These markers were readily visible in the positive transparencies and were used as reference positions. After acquisition of the photography, videography of the test fields was acquired from 3050 m using the system described by Everitt et al. (1991). Wavelength sensitivity intervals are as given in Table 2.

Digital Data Extraction

The positive photographic transparencies were digitized using an Eikonix model EC 78 /99 digital imaging camera. Red, green, and blue dichroic filters from Optical Coating Laboratories, Inc. were used successively on the camera to produce B-bit digital count (DC) readings that characterized the film's NIR, red, and green wavelength responses (Table 2). Pixel size ranged from 1.0 m^2 to I.4 m^2 ground area per digital value.

The videography images for each field in each wavelength, as recorded on 400 horizontal line resolution Super-VHS recorders, were "grabbed" with a Matrox digitizing board and IMAGER software and saved. The B-bit digital counts acquired by this procedure represented a ground area II-12 m^2 in size.

The data extracted for each field were stored on floppy disks. Then the data from all bands of all systems were registered to the NIR band of the photography for each field using PCI, Inc. EASI /PACE image processing software. The registered images were saved. The coordinates of the sample sites, in meters, were converted to pixel coordinates in the NIR photographic image and overlaid on images for the other bands. The digital counts for the sample sites for each data type were then extracted.

Computation of Vegetation Indices

NDVI was calculated from digital counts as

$$NDVI = (NIR - RED) / (NIR + RED). \quad (2)$$

GVI3 was obtained by the procedure of Jackson (1983) for the three bands of each system except that the greenness of the bare soil was subtracted from the greenness calculated for each pixel (Wiegand et al., 1991). The resulting GVI3 equations for photography (p) and videography (u) were

$$GVI3_p = -0.179\,Green - 0.397\,Red + 0.900\,NIR - 39.32, \quad (3a)$$

$$GVI3_v = -0.076\,Green - 0.383\,Red + 0.920\,NIR + 7.01 \quad (3b)$$

(fields 2C, 3C, and 9E),

$$GVI3v = 0.015\,Green - 0.224\,Red + 0.975\,NIR - 46.98 \quad (3c)$$

(field 9A).

A separate equation was needed for the videography

Table 3. Correlations of PH and EC1 by Field with Spectral and Ground Truth Variables

	Field							
	2 c		3 c		9A		9E	
Variable	PH (cm)	EC1 (dS/m)	PH (cm)	EC1 (dS/m)	PH (cm)	EC1 (dS/m)	PH (cm)	EC1 (dS/m)
				A. Photography (r^a)				
NIR	– 0.46	0.58	– 0.33	0.10	– 0.59	0.50	– 0.38	0.46
Red	– 0.69	0.77	– 0.57	0.47	– 0.70	0.60	– 0.90	0.78
Grn	– 0.67	0.75	– 0.55	0.45	– 0.71	0.62	– 0.90	0.78
NDVI	0.77	– 0.73	0.63	– 0.53	0.72	– 0.57	0.90	– 0.68
GV13	0.61	– 0.57	0.52	– 0.69	0.03	– 0.03	0.89	– 0.70
				B. Videography				
NIR	0.54	– 0.46	0.35	– 0.41	0.43	– 0.21	0.80	– 0.61
Red	– 0.68	0.72	– 0.59	0.43	0.73	0.62	– 0.88	0.71
Grn	– 0.66	0.71	– 0.50	0.36	-0.69	0.64	– 0.83	0.69
NDVI	0.70	– 0.69	0.60	– 0.46	0.74	– 0.56	0.85	– 0.67
GV13	0.69	– 0.68	0.59	– 0.51	0.61	– 0.40	0.86	– 0.67
				C. Ground Truth				
EC0	– 0.62	0.80	– 0.45	0.68	– 0.33	0.47	No data	
EC1	– 0.72	1 .00	– 0.65	1 .00	– 0.64	1 .00	– 0.82	1 .00
EC2	– 0.72	0.91	– 0.56	0.75	– 0.35	0.62	– 0.78	0.82
PBARE	– 0.73	0.81	– 0.68	0.74	– 0.72	0.55	– 0.85	0.75
[a] r for p = 0.05:	0.14		0.16		0.14		0.20	
[a] r for p = 0.01:	0.18		0.21		0.18		0.25	

data for field 9A because its reference soil plane differed from that of the other fields.

Data Analysis

The above procedures resulted in two distinct data sets. One set consisted of the plant, soil, and spectral data for the sample sites, whereas the other was the digital spectral data for all pixels in each field (the whole population) in the photography and videography.

The sample site data were used to determine how the observations interrelated, to examine them for outliers, and to select a single depth of salinity measurements to characterize the sample sites. Scatter plots of data pairs and correlation matrices were the main procedures used. Spectral and salinity observations for the sample sites were also submitted to multiple regression analyses to produce equations for estimating EC1 for every pixel in each field.

Those equations by field for photography were:

$$2C: EC1_p = 2.11 - 0.031\ NIR + 0.131\ Red - 0.073\ Grn,\ R^2 = 0.68, \quad (4a)$$

$$3C: EC1_p = 6.48 - 0.056\ NIR + 0.038\ Red + 0.016\ Grn,\ R^2 = 0.64, \quad (4b)$$

$$9A: EC1_p = 2.64 - 0.020\ NIR - 0.057\ Red + 0.138\ Grn,\ R^2 = 0.39, \quad (4c)$$

$$9E: EC1_p = 5.49 - 0.027\ NIR + 0.182\ Red - 0.094\ Grn,\ R^2 = 0.64. \quad (4d)$$

The corresponding equations for the videography were

$$2C: EC1_v = -1.65 - 0.004\ NIR + 0.033\ Red + 0.029\ Grn,\ R^2 = 0.59, \quad (5a)$$

$$3C: EC1_v = 12.08 - 0.083\ NIR + 0.010\ Red + 0.020\ Grn,\ R^2 = 0.39, \quad (5b)$$

$$9A: EC1_v = -1.71 - 0.006\ NIR + 0.032\ Red + 0.068\ Grn,\ R^2 = 0.46, \quad (5c)$$

$$9E: EC1_v = 8.15 - 0.054\ NIR + 0.092\ Red + 0.026\ Grn,\ R^2 = 0.59. \quad (5d)$$

The whole field data for the digitized photography were analyzed in two ways. First, unsupervised classifications of the digital counts into eight spectral categories were performed for each field with PCI, Inc. software. One category was a small threshold group of outlier pixels while seven were meaningful categories. The procedure used migrating means and four-dimensional histograms to develop and separate spectral classes and generated mean and covariance matrices for each class (or category). Individual pixels were classified by a maximum likelihood ratio criterion using the statistics generated for each class. The procedure provided a report that gave the digital count means for each of the three bands for each category and the number of inclusions of individual and small "islands" of pixels in displays of the classifications. The individual pixel classifications were smoothed by the median DC of the 3 x 3 array

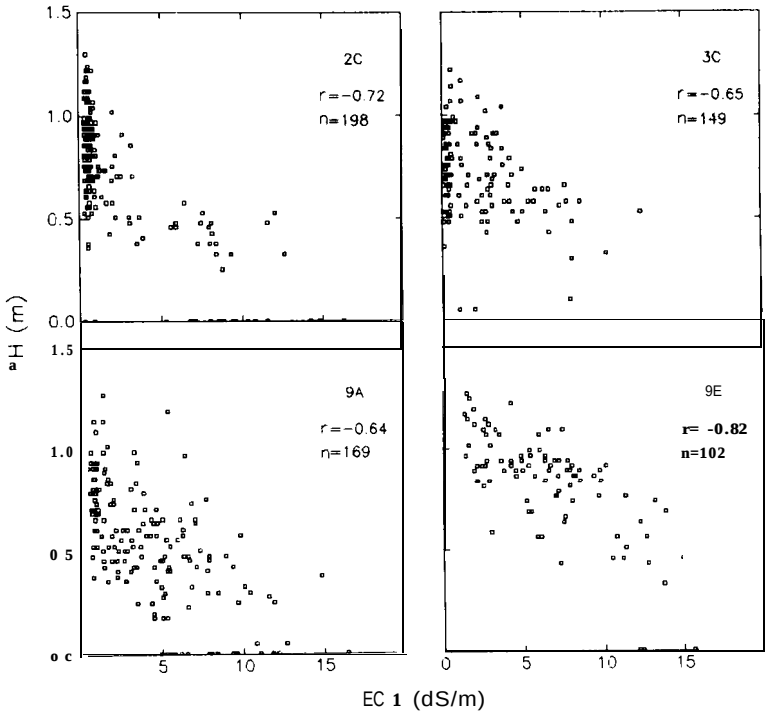

Figure 1. Plant height (PH) vs. salinity of the surface 30 cm of soil (ECl) for four fields (2C, 3C, 9A, 9E).

surrounding each pixel. These smoothed spectral classifications were saved, the report was again generated, and the results were color-coded, displayed, and photographed.

In the second analysis for each field, the multiple regression equations from the sample sites [Eqs. (4) and (5)] were used to estimate the mean salinity of each spectral class from the mean digital count for each classification category. The EC1 values at the midpoint between categories were used to set the ranges in each salinity class. Equation (4) was then used to assign salinity classes to the approximately 100,000 photographic pixels in each field. These salinity classifications were saved, and the number of pixels in each category was listed. Color codes corresponding to those for the unsupervised spectral classifications were assigned and the images were displayed and photographed.

The results from the spectral and salinity classifications were submitted to a matrix coincidence analysis using the PCI, Inc. subroutine, MAT. The procedure sorted pixels by a cross-classification procedure into a matrix where each element of the matrix corresponded to overlapping categories from the spectral classification (image 1) and the salinity classification (image 2). Pixels along the diagonal of the matrix were cross-classified into the same category in both images, while increasing distance from the diagonal indicated increasing disparity in category correspondence between images.

For publication purposes the spectral and electrical conductivity image classifications were converted from PCI, Inc. software raster files to the personal computer version of ARC / INFO vector files. The vector files were used to create line drawing classification maps. The data were smoothed twice with a 5 x 5 pixel array mode filter before the figures were produced.

RESULTS

Plant, Soil and Spectral Interrelationships

Table 3 summarizes the correlations of both plant height (PH) and electrical conductivity of the O-30 cm depth (ECl) by field with the spectral measurements (individual bands and the vegetation indices NDVI and GVI3) and the other ground measurements, percent bare (PBARE) and electrical conductivity of the O-2 cm (ECO) and 30-60 cm (EC2) soil depths.

As shown in part C of Table 3, electrical conductivity of the surface 30 cm of the soil (ECl) correlated more closely with plant height than either EC0 or EC2. Therefore, EC1 was chosen as the measurement of soil salinity. Correlations of the natural logarithm of EC1 (In ECl) with the plant and spectral variables were typically 0.02-0.08 lower than those for ECl. Therefore, we discontinued investigating nonlinear salinity effects.

In Table 3, magnitudes of the coefficients were similar, but opposite in signs for PH and EC1 versus the spectral variables. For field 2C, EC1 related somewhat more closely to the photographic and videographic spectral observations than did PH, but for fields 3C, 9A, and 9E the reverse was true. The negative correlation between the NIR band for photography and PH resulted

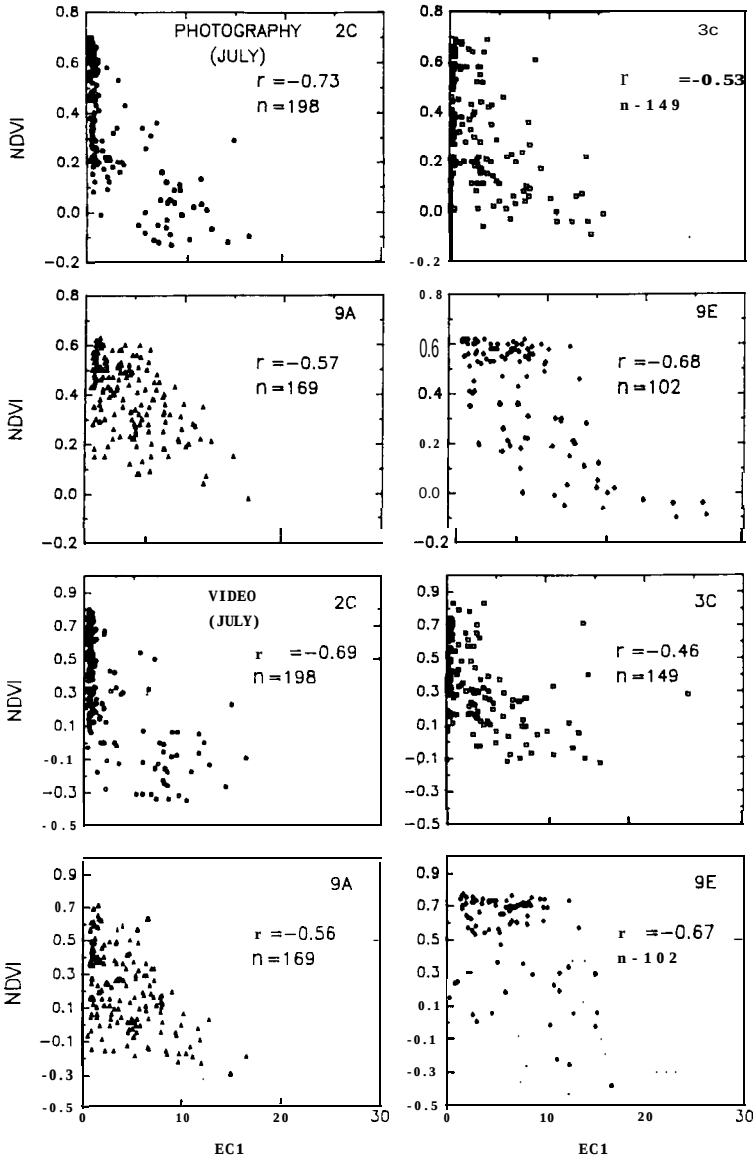

Figure 2. Normalized difference vegetation index (NDVI) vs. EC1 for each of four fields from photography (upper set) and videography (lower set).

from the inverse relation between plant vigor and digital counts in the digitization of the photography. From Table 3 results we decided to emphasize NDVI as the spectral characterizer of plant growth and soil salinity conditions.

Scatter diagrams between plant height and EC1 are displayed by field in Figure 1. Figure 2 displays the relation between NDVI and EC1 by field for both the photographic and videographic observations. The correlation coefficients were slightly better for the photography than the videography. Summaries of the digital count means and standard deviations for the bands of all instruments by field (not shown) indicated that the coefficient of variation (SD. x 100 / mean) for the NIR band of the videography was less than 25% compared with typically 60% for the other video bands and all bands of the photography. When the NIR video band scene was displayed on a CRT, it produced an image with low contrast. In retrospect, the 0.5 neutral density filter may have overly dampened the response of the sensor in the NIR video camera.

The correlation coefficients presented in Figures 1 and 2 and Table 3 are mostly far in excess of those required for significance at the p = 0.01 level, but they are low enough to indicate either errors in observations, less than optimum sampling, or dependent variables that were functions of additional independent variables. Figure 2 indicates there were a few outliers in the spectral observations but the correlation coefficients are remarkably consistent between the completely independent data sources, photography and videography. In Figure 1, instances where the plant height (PH) is zero at soil salinity less than 10 dS m^{-1} is due to skips in the plant row right at the sample site. The experimental

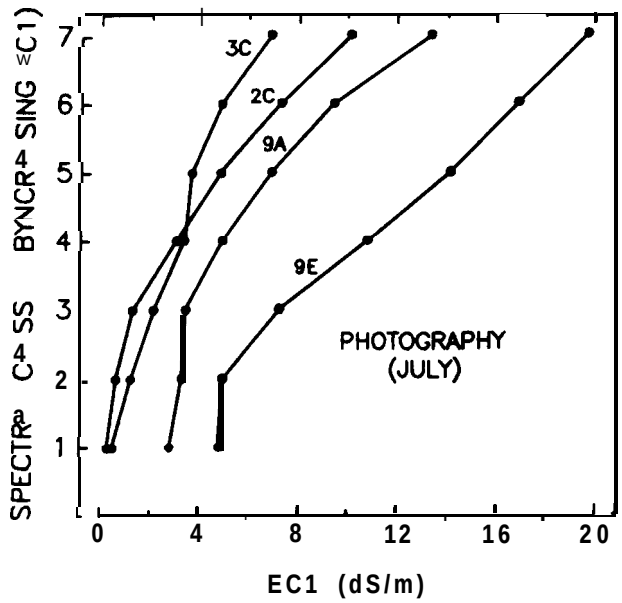

Figure 3. Spectral class number for each field in order of increasing salinity versus mean salinity of each class. Spectral class mean digital counts were inserted into Eqs. (4a)-(4d) to estimate the mean salinity of each class.

data for each field were reanalyzed after deleting five to seven sites where average plant height in the 10 m x 10 m area surrounding the sample sites was far different from the zero reported at the sample site and one to three spectral observations. The number of observations deleted per field ranged from six to 10. The correlations with PH improved by only 0.06-0.08 because the number of observations was large. The correlations with the individual bands improved much more than did the correlations with the vegetation indices. Because operational applications would have to tolerate realistic inconsistencies, Figures 1 and 2 and Table 3 are presented for the data sets with no sites deleted. However, Eqs. (4) and (5) are based on the data with six to 10 observations deleted out of 102 to 198 per field in order to improve the estimates of salinity everywhere in the field from the sample site data.

Spectral and Salinity Classifications

Spectral and salinity classifications are reported for only the full resolution photographic data since Figure 2 indicates that photographic and videographic observations should support very similar conclusions about plant growth and salinity. Figure 3 displays the spectral classes for each field versus mean estimated EC1 from Eqs. (4a)-(4d). The salinity ranges covered by the spectral classes agreed well with the measured salinity ranges in Figure 2. However, the wider the salinity range, the higher the salinity of the least saline class in keeping with a wider salinity interval per category to produce the same number of spectral categories (eight) per field as salinity increased. Although more spectral categories could have been requested in the unsupervised classifications, we used eight uniformly across all fields to keep the salinity categories to a practical number. The EC1 measurements at some sample sites and the appearance of the plants in the CRT displays of the digitized photography disagreed at some sample sites for field 9A, supporting the lower coefficient of determination (R^2) of 0.39 in Eq. (4c) for this field. The lower R^2 values from the videography [Eqs. (5a)-(5d)] compared with Eqs. (4a)-(4d) for photography indicate more reliable estimates of EC1 from the digitized photography than the videography in agreement with the PH results of Figure 1.

Table 4 summarizes the percentage of the area in each field and the EC1 range for the unsupervised spectral classifications of fields 2C, 3C, and 9E. The boundary between adjacent salinity categories in Table 4 was obtained by averaging the mean EC1 for adjacent salinity classes, as calculated by inserting the mean digital count for each spectral band by class in Eqs. (4a)-(4d). Field 9A was not included in Table 4 because

Table 4. Percent of Field Area and EC1 Range in Each Spectral Class for Fields 2C, 3C, and 9E

	2 c		3 c		*9E*	
Class Code	Field *Area (%)*	*EC1* Range *(d S/m)*	Field *Area (%)*	*EC1* Range *(d S/m)*	Field *Area (%)*	*EC1* Range *(dS/m)*
0[a]	2.3	–	3.5	–	1.2	_
1	23.6	< 0.5	25.2	< 0.9	42.1	< 4.8
2	11.7	0.5-0.8	14.6	0.9-1.6	10.6	4.8-6.0
3	19.3	0.8-2.2	15.9	1.6-2.4	16.1	6.0-8.9
4	15.7	2.2-4.0	14.6	2.4-3.3	10.4	8.9-12.3
5	12.4	4.0-6.2	8.1	3.3-4.2	8.1	12.3-15.5
6	9.2	6.2-8.8	10.7	4.2-5.9	6.7	15.5-18.4
7	5.8	> 8.8	7.4	> 5.9	4.8	> 18.4
Total	100		100		100	

[a] Class 0 **is composed of pixels that do not fit the pattern for any of the established classes.**

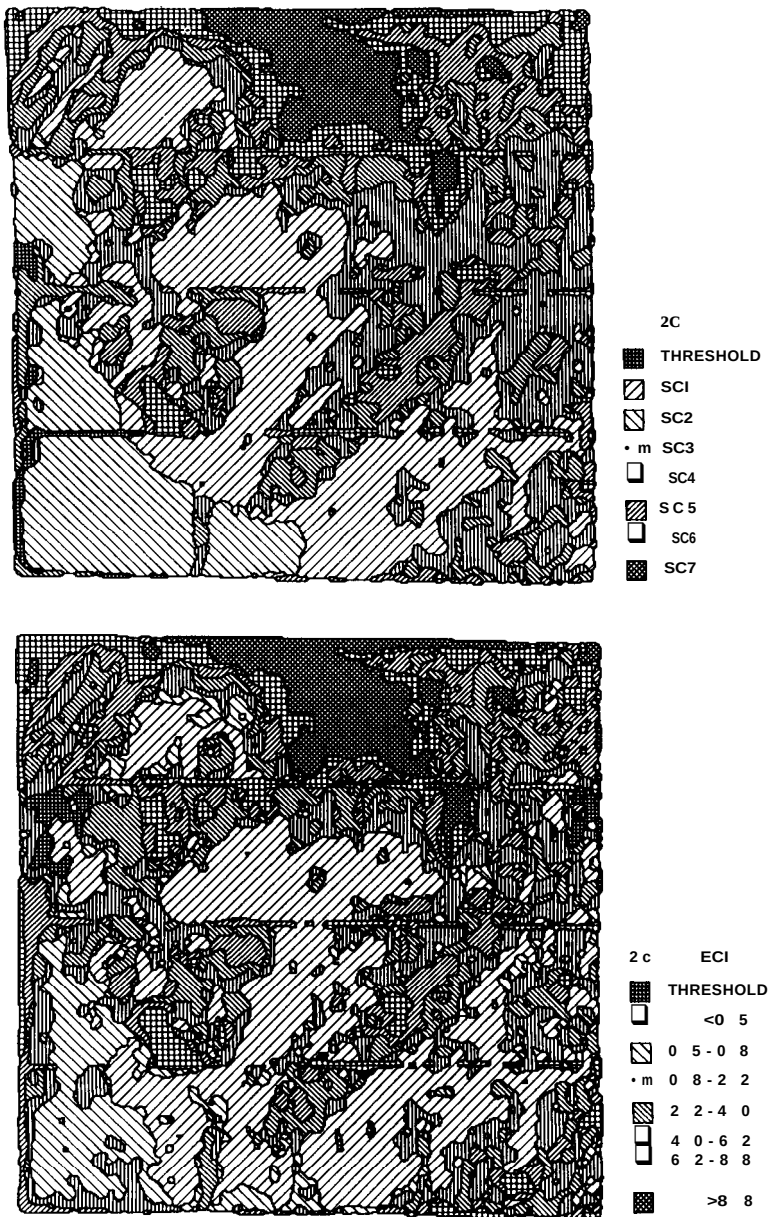

Figure 4. Spectral classification (SC) map (upper) and predicted salinity (ECl) map (lower) for field 2c.

of uncertainty in Eq. (3c). In Table 4, the zero or threshold class consisted of pixels with erratic DC that defied classification. Those pixels often occurred at field edges. According to Table 4, 70.3% of the area in field 2C had EC1 < 4,78.4% of the area in 3C had EC1 < 4.2, and 42.1% of 9E had EC1 < 4.8.

Figure 4 displays the patterns of the spectral classification (SC) and the salinity classification (ECl), based on Eq. (4a), for field 2C in upper and lower parts of the figure, respectively. In this field three drain lines, revealed by the color contrast between the backfill and surface soils, cross the field and sometimes interrupt the patterns. The cross-hatch symbols corresponding to increasing (or decreasing) salinity usually occurred adjacent to each other as one proceeds from most saline to least saline, or vice versa. The data for both parts of Figure 4 were smoothed twice before the maps were produced. The correspondence between the two maps is evident and is especially good between the saline areas along the top center of the maps. The least saline area in both maps also forms a generally upper left to lower right pattern.

The matrix analyses provided another way to examine the agreement / disagreement between the spectral and salinity maps. That analysis for field 2C is summarized in Table 5, where pixels along the diagonal were classified into the same class by both procedures. For this field 64.9% of the classifications coincided. The

Table 5. Number of Pixels in Each Salinity Class and Percentage in Each Salinity Class Relative to Total Number of Pixels in Each Spectral Class for Field 2C

No. *Pixels* / *EC1 Class*	*Spectral Class (% of Class)*						
	1	2	3	4	5	6	7
1	24,659 (76.2)	4,567 (27.7)	5,260 (19.4)	111 (0.5)	25 (0.1)	16 (0.0)	1 (0.0)
2	4,424 (13.7)	8,681 (52.6)	3,644 (13.5)	71 (0.3)	5 (0.0)	5 (0.0)	0 (0.0)
3	3,134 (9.8)	3,239 (19.6)	13,775 (50.9)	5,129 (24.5)	178 (1.0)	33 (0.3)	1 (0.0)
4	106 (0.0)	17 (0.0)	4,175 (15.4)	11,663 (55.8)	4,857 (28.2)	142 (1.1)	1 (0.0)
5	18 (0.0)	0 (0.0)	148 (0.5)	3,758 (18.0)	9,148 (53.2)	2,751 (21.3)	2 (0.0)
6	7 (0.0)	0 (0.0)	57 (0.2)	188 (0.9)	2.990 (17.4)	8,976 (69.4)	329 (4.1)
7	0 (0.0)	0 (0.0)	1 (0.0)	0 (0.0)	11 (0.0)	1,008 (7.8)	7,671 (95.8)
	32,348	16,504	27,060	20,919	17,203	12,931	8,005

matrix analysis showed that an additional 30.3% of the pixels were confused with the adjacent higher or lower class. This was encouraging since point samples of salinity were interpolated to represent unsampled areas. Variation also existed in the photographic digitizations due to skips in the plant stands, changes in soil type (color) across fields, and film exposure variations within frames. For comparison, the percent coincidence was 37.8% for field 3C, 68.4% for field 9A, and 62.1% for field 9E, while the percentage of pixels assigned to adjacent categories was 26.4, 26.8, and 37.1%, respectively, for fields 3C, 9A and 9E. Field 9A had fewer rapid changes in salinity and the coincidence of classification was good, even though estimates of salinity for the sample sites [Eq. (4c)] were imprecise.

Salinity-Yield Relations

The economic impact of salinity is through crop yield reduction and the costs of reclamation. Thus, if a relation were developed between yield and the vegetation indices, the crop yield categories could be mapped directly and economic costs estimated. Therefore, cotton boll counts taken at a fraction of the sampling sites were used to develop yield (NDVI) and yield (ECl) equations after deleting the same data as deleted in developing Eqs. (4) and (5) a few sites with outlier boll counts. These relations are the left-side and first right-side terms of Eq. (1) displayed in Figures 5 and 6, respectively, for fields 2C, 3C, and 9E.

Field 9A had NDVI and EC1 values similar to the other fields and was not included in Figures 5 and 6 because higher boll counts caused yields to be 300-400 kg ha^{-1} higher for a given NDVI than for the other fields. The simple product moment correlation coefficients (r), which were 0.73 for the photographic and 0.72 for the videographic data, indicate that a little over half the variation in yield was accounted for by instantaneous spectral observations midway in the fruiting (boll set) period. In contrast, in Figure 6, the r of – 0.52 indicates that soil salinity accounted for only 27% of the yield variation. Consequently, use of the plants and particularly their canopy development to integrate the salinity effects was clearly superior to use of the salinity measurements directly.

The equations in Figure 5 and statistics for them show that there were 97 ± 13 and 85 ± 12 kg ha-' increases in yield for each 0.1 increase in NDVI, and NDVI,, respectively. The standard error of the estimate of yield was I92 kg ha-' and 197 kg ha-' for the photographic and videographic data, respectively, or 18% of the yield range. Likewise, the equation on Figure 6 estimates a 43 ± 10 kg ha-' decrease in lint cotton yield for each unit increase in electrical conductivity of the surface 30 cm of the root zone. Since the market price of cotton is currently about $1.20 per kg, the losses (or gains) in income can be calculated for given changes in NDVI or salinity-as from the average values that were 3.2 dS m^{-1} for ECl, 0.43 for NDVI,, and 0.50 for NDVI,.

The inverse of the second right-hand side term of Eq. (l), EC(NDVI) is shown for each of the four fields in Figure 2. Salinity was expected to be the main source of the variation in plant growth. Since the functions in Figures 5 and 6 both estimate yield, they were set equal

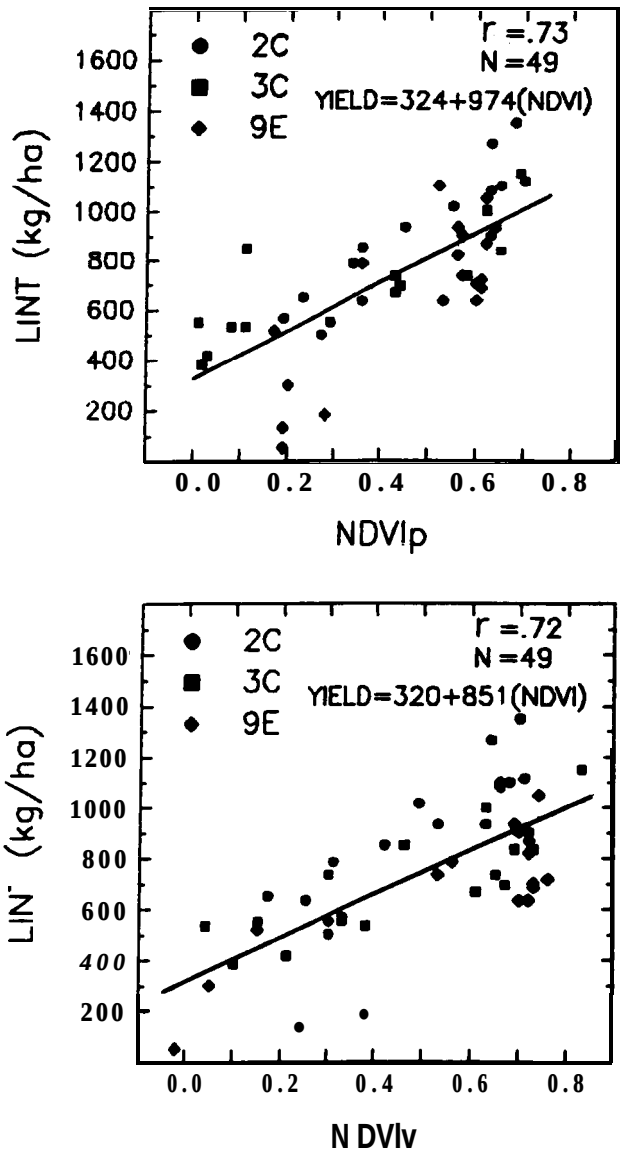

Figure 5. Estimates of cotton lint yield from NDVIp (photography) and NDVIv (videography) for fields 2C, 3C, and 9E.

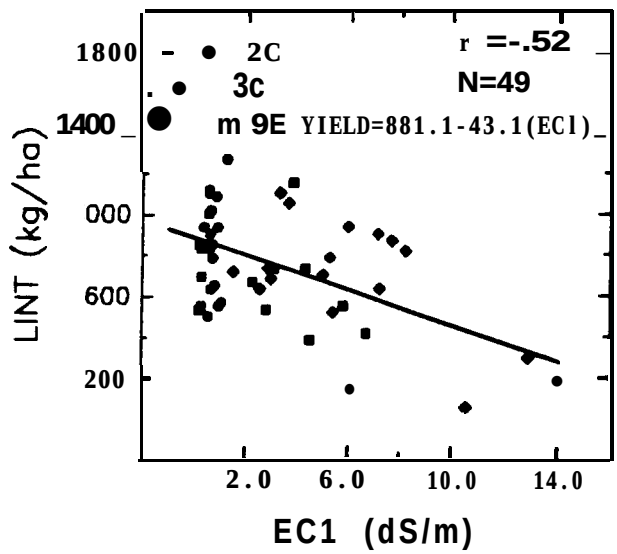

Figure 6. Estimates of cotton lint yield from electrical conductivity of the surface 30 cm of soil (ECl) for fields 2C, 3C, and 9E.

to each other and solved for NDVI, (photography) in terms of ECl. That expression was

$$\text{NDVI}, = 0.57 - 0.044(\text{ECl}). \quad (6)$$

For EC1 values of 1 dS $/m^{-1}$, 10 dS $/m^{-1}$ and 20 dS $/m^{-1}$, Eq. (6) predicts corresponding NDVI values of 0.53, 0.22, and – 0.31. For NDVI, values of – 0.30, 0.1, and 0.5, the corresponding EC1 values are 19.7 dS/m-i, 12.8 dS $/m^{-1}$, and 1.6 dS $/m^{-1}$. Equation (6) represents the photography data displayed in Figure 2 rather well.

DISCUSSION

The lasting value of this work is that it demonstrates how ground measurements, aerial (or satellite) spectral observations, and image analysis can be used jointly to map cropped fields for the extent or severity of salinity. Unsupervised spectral classification provides an unbiased method of determining spectrally distinctive categories of response to salinity. Then the multiple regression equations developed from the salinity and spectral data at sample sites defines the salinity of the spectral categories. Because the spectral data, illustrated herein with photography and videography, contain the whole population of the field, salinity maps can be produced of the fields.

If geographic information systems are in place, land uses not of interest as well as roadways, turnrows, canals, drains, borrow ditches, farmsteads, and other non-cropped areas can be masked out of the spectral data. Then, if plant and soil salinity have been measured at representative sites, the procedure could be applied to several square kilometers of the landscape at once. In this study we used the fields as replications of the procedure. They were separated geographically within the 39 km^2 study area and were subjected to differences in soils and management practices, as well as differences in distribution of salinity with depth in the soil profiles.

The data for the three fields could have been pooled and analyzed as one data set. However, our mind set at the time the work was done was that five to seven salinity intervals are optimal and meaningful. Within this criterion, our experience for cotton is that dS m^{-1} ranges of approximately $\leqslant 4$, 4-8, 8-12, 12-16, 16-20,

and *>20* are appropriate. Therefore, we used eight-category classifications for all fields which resulted in a small threshold class and seven useable categories (Table 4). In retrospect, a 16-category or 32-category unsupervised spectral classification of the pooled data for the three fields could have been done, but that number of salinity categories is unnecessary and difficult to interpret.

Equation (1) the spectral components identity applicable to plant response to soil salinity, guides the user to the important relationships: yield as functions of vegetation indices and soil salinity, and, for predictive purposes, soil salinity as a function of vegetation indices. Once developed, these relationships provide the economic estimates to justify reclamation efforts, and then a way to monitor progress of reclamation. If spectral-yield relations have been developed, then yield maps useful for prescription farming or for depicting yield losses can also be produced.

The yield relationships are climate dependent (Wiegand and Richardson, 1984; 1990) and are also dependent on the time of collection of the boll counts for estimating yield. In this San Joaquin Valley of California study, the boll counts were made at the end of July or about midway through the boll set period. In a south Texas study (Wiegand et al., 1992) boll counts and videography taken after bolls had begun to open gave the equation

$$\text{Yield} = 246 + 1572\ (\text{NDVI},),\ n = 35\ r = 0.78, \quad (7)$$

where lint yield is in the same units as in this study (kg ha^{-1}). This equation has about the same intercept but a larger slope than the equation for videography in Figure 5.

The variation among fields in some responses was a concern in this study. All the fields gave similar responses in NDVI for both the photography and videography. However, field 9A had 300-400 kg ha-' higher yields and in field 9E the plants grew taller at the higher salinities (Fig. 1) than in the other fields. We do not know why. Variations in boll counts were almost certainly vulnerable to irregularities in stand among l-m-long row segments. Superimposed on those variations were others associated with variable management among fields and experimental sampling error. Consequently, the reader should not dwell on them ("throw the baby out with the bath water"), but rather the ideas (the "brain children") of the study.

CONCLUDING REMARKS

In this study there were moderate correlations among spectral observations (individual bands and vegetation indices) for two systems, the plant observations height and (l-cover), and the soil salinity measurements. We have also demonstrated that unsupervised spectral classifications identify the plant growth categories associated with soil salinity, and that spectral data for sites sampled for salinity can be used to estimate the salinity of all pixels in the field. Reports generated from the spectral and salinity classifications provide estimates of the percent of the field in each salinity category, and the classifications can be mapped. These information forms are very practical for managing individual fields and monitoring salinity changes in them. The relationships expressed by Eq. (1) and illustrated by the equations in Figures 5 and 6 can be used to estimate economic losses from salinity (or the value of reclamation).

We *have many colleagues to thank: Rene Davis for acquisition of the photography and videography; Scott Lesch for clarifying sampling procedures, preparing the sample site data sets, and performing the photographic film digitizations; Ricardo Villarreal for conducting the spectral* and *salinity classifications and matrix analyses; Arthur J. Richardson for deriving equations for locating sample sites and for matrix analysis interpretation; Romeo Rodriguez and Wayne Swanson for preparation of figures; and Carol Harville and Saida Cardoza for manuscript preparation.*

REFERENCES

Carter, D. L. (1975) Problems of salinity in agriculture, in *Ecological Studies, Analysis and Synthesis, Vol. 15, Plants in Saline Environments* (A. Poljakoff-Mayber and J. Gale, Eds.), Springer-Verlag, New York, pp. 25-35.

Everitt, J. H., Gerbermann, A. H., and Cuellar, J. A. (1977), Distinguishing saline from non-saline rangelands with SKYLAB imagery, *Photogramm. Eng. Remote Sens. 43:1041-1047.*

Everitt, J. H., Escobar, D. E., Gerbermann, A. H., and Alaniz, M. A. (1988) Detecting saline soils with video imagery, *Photogramm.* Eng. *Remote Sens.* 54:1283-1287.

Everitt, J. H., Escobar, D. E., and Noriega, J. R. (1991) A high resolution multispectral video system, Geocarto *Int.* 6:45-51.

Jackson, R. D. (1983) Spectral indices in n-space, *Remote Sens.* Environ. 13:409-421.

Kauth, R. J., and Thomas, G. S. (1976) The Tasseled Cap-a graphic description of the spectral temporal development of agricultural crops as seen by LANDSAT, Proc. Symp. Machine Proc. Remotely Sensed Data, IEEE, New York, pp. 41-49.

Lesch, S. M., Rhoades, J. D., Lund, L. J., and Corwin, D. L. (1992), Mapping soil salinity using calibrated electromagnetic measurements, Soil Sci. Soc. Am. J. 56:540-548.

Myers, V. I., Ussery, L. R., and Rippert, W. J. (1966), Photogrammetry for detailed detection of drainage and salinity problems, Trans. *ASCE 6(4):332-334.*

Rhoades, J. D. (1982), Soluble salts, in *Methods of* Soil Analysis,

Part 2, 2nd ed. Agronomy 9 (A. L. Page, Ed.), Am. Soc. of Agronomy, Madison, WI, pp. 167-178.

Richards, L. A. (Ed.), (1954), ***Diagnosis and lmprovement of*** Saline ***and Alkali Soils,*** U.S. Dept. Agric. Handbook No. 60, Government Printing Office, Washington, DC.

Richardson, A. J., and Wiegand, C. L. (1977). Distinguishing vegetation from soil background information, ***Photogramm.*** Eng. 43:1541-1552.

Sharma, R. C., and Bhargava, G. P. (1988) Landsat imagery for mapping saline soils and wetlands in north-west India, ***lnt. J. Remote Sens. 9:39-44.***

Szabolcs, I. (1989) ***Salt-Affected Soils,*** CRC Press, Boca Raton, FL, 274 pp.

Tanji, K. K. (1990), The nature and extent of agricultural salinity problems, in ***Agricultural Salinity Assessment and Management,*** ASCE Manuals and Reports on Engineering Practice No. 71 (K. K. Tanji, Ed.), Am. Soc. Civil Eng., New York, pp. l-17.

Tucker, C. J. (1979) Red and photographic infrared linear combinations for monitoring vegetation, ***Remote Sens. Environ. 8:127-150.***

Wiegand, C. L., and Richardson, A. J. (1984) Leaf area, light interception, and yield estimates from spectral components analysis, Agron. J. 76:543-548.

Wiegand, C. L., and Richardson, A. J. (1987), Spectral components analysis. Rationale, and result for three crops. Int. J. ***Remote Sens. 7:1011-1032.***

Wiegand, C. L., and Richardson, A. J. (1990) Use of spectral vegetation indices to infer leaf area, evapotranspiration and yield: I. Rationale, ***Agron. J. 82:623-629.***

Wiegand, C. L., Learner, R. W., Weber, D. A., and Gerbermann, A. H. (1971), Multibase and multiemulsion space photos for crops and soils, ***Photogramm.*** Eng. 37:147-156.

Wiegand, C. L., Richardson, A. J., Escobar, D. E., and Gerbermann, A. H. (1991) Vegetation indices in crop assessments, ***Remote Sens. Enuiron. 35:105-119.***

Wiegand, C. L., Everitt, J. H., and Richardson, A. J. (1992) Comparison of multispectral video and SPOT-l HRV observations for cotton affected by soil salinity, ***Int. J. Remote Sens. 13:1511-1525.***

Wiegand, C. L., Escobar, D. E., and Lingle, S. E. (1993), Detecting growth variation and salt stress in sugarcane using videography, in ***Proc. 14th Biennial Workshop, Aerial Photography and Videography in the Plant Sciences,*** Logan UT, 25-28 May, Am. Soc. Photogramm. and Remote Sens., Bethesda, MD, forthcoming.